




RESEARCH ARTICLE | FEBRUARY 14 2022

Beating the limitation of the Néel temperature of FeO with antiferromagnetic proximity in FeO/CoO

A. Kozioł-Rachwał ; M. Szpytma; N. Spiridis ; K. Freindl ; J. Korecki; W. Janus; H. Nayyef; P. Drózdź; M. Ślęzak; M. Zajac; T. Ślęzak




Appl. Phys. Lett. 120, 072404 (2022)


<https://doi.org/10.1063/5.0082729>



CrossMark




Lock-in Amplifier



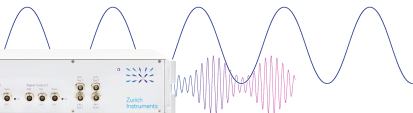
Zurich
Instruments

[Find out more](#)



Boxcar Averager

Boost Your Optics and
Photonics Measurements



Beating the limitation of the Néel temperature of FeO with antiferromagnetic proximity in FeO/CoO

Cite as: Appl. Phys. Lett. **120**, 072404 (2022); doi: [10.1063/5.0082729](https://doi.org/10.1063/5.0082729)

Submitted: 17 December 2021 · Accepted: 27 January 2022 ·

Published Online: 14 February 2022



View Online



Export Citation



CrossMark

A. Kozioł-Rachwał,^{1,a)} M. Szpytma,¹ N. Spiridis,² K. Freindl,² J. Korecki,² W. Janus,¹ H. Nayyef,¹ P. Drózd,¹ M. Ślęzak,¹ M. Zajac,³ and T. Ślęzak¹

AFFILIATIONS

¹Faculty of Physics and Applied Computer Science, AGH University of Science and Technology, al. Mickiewicza 30, 30-059 Kraków, Poland

²Jerzy Haber Institute of Catalysis and Surface Chemistry, Polish Academy of Sciences, 30-239 Kraków, Poland

³National Synchrotron Radiation Centre SOLARIS, Jagiellonian University, Kraków, Poland

^{a)}Author to whom correspondence should be addressed: akozioł@agh.edu.pl

ABSTRACT

In our study, we investigate the influence of the proximity of an antiferromagnetic CoO layer on magnetic properties of ultrathin wüstite (FeO) films. Comparative Mössbauer spectroscopy measurements for MgO/FeO/MgO(001) and MgO/FeO/CoO/MgO(001) show that the neighboring CoO layer can significantly enhance the ordering temperature (T_N) of wüstite. Importantly, we find that the proximity of antiferromagnetic CoO strongly influences the exchange interaction at the Fe/FeO interface in the Fe/FeO/CoO heterostructure. We observe a 500% enhancement in the exchange bias field and a double increase in the blocking temperature compared to the Fe/FeO bilayer. Our results show that the limitation of the low ordering temperature of a seemingly application-useless antiferromagnet can be overcome by antiferromagnetic proximity.

© 2022 Author(s). All article content, except where otherwise noted, is licensed under a Creative Commons Attribution (CC BY) license (<http://creativecommons.org/licenses/by/4.0/>). <https://doi.org/10.1063/5.0082729>

Antiferromagnets (AFMs) are promising candidates for future spintronic materials because of their unique properties. Unlike ferromagnets (FMs), AFMs are robust against magnetic perturbations and do not create stray fields, which are beneficial for the ultimate downsize scalability of magnetic memory devices.^{1,2} The possibility of manipulating the antiferromagnetic Néel vector via field-like spin-orbit torques in AFMs^{3,4} or spin-orbit torques in AFM/heavy metal bilayers,⁵ together with anisotropic and spin Hall magnetoresistance (SMR) effects^{6,7} observed in AFMs, has revealed the feasibility of using antiferromagnets as active elements in spintronics devices. Unfortunately, a wide group of AFM materials seems to be useless for applications because of the low ordering temperature (Néel temperature, T_N), above which the long-range antiferromagnetic order vanishes. The restriction of low T_N can be overcome using the magnetic proximity effect (MPE).⁸ The MPE is attributed to the interfacial interaction between magnetic layers that possess different ordering temperatures and/or different types of magnetic ordering. The consequence of the MPE can be a change in the magnetic ordering temperature of the adjacent layers and/or modulation of their spin configuration. Previous experimental studies have confirmed the possibility of

modulating the magnetic properties of materials owing to the MPE.⁹ The MPE is responsible for the induction of the magnetic moment in the PM in FM (AFM)/paramagnet (PM) bilayers.^{10–14} In FM (ferromagnet-FIM)/AFM bilayers, the proximity effects are responsible for a change in the ordering temperature in the FM, FIM, and AFM layers.^{15–18} Comparative studies of the magnetic properties of FM nanoparticles embedded in PM and AFM matrices demonstrated an impressive enhancement in the superparamagnetic blocking temperature of particles in contact with AFM.¹⁹ Similarly, the thermal stabilization of magnetization due to MPE has been proven for Co and Fe₃O₄ clusters within the ferromagnetic NiFe matrix.^{20,21} A single ordering temperature with a value between T_N 's of the sub-layers was obtained for short-repeat-distance superlattices consisting of two AFMs due to the MPE.^{22,23} Additionally, Carey *et al.* showed that the magnetocrystalline anisotropy of the Co and Ni monoxide layers strongly depends on the interlayer coupling in the AFM multilayers.²⁴ There have been only a few studies on proximity effects in AFM/AFM bilayers. Zhu *et al.* and Li *et al.* investigated the magnetic properties of NiO/CoO/MgO(001) and CoO/NiO/MgO(001) structures using x-ray magnetic linear dichroism (XMLD).^{25,26} They reported an

enhancement in the Néel temperature of CoO due to the MPE and showed that interfacial coupling could induce a spin reorientation transition (SRT) in NiO. Yang *et al.* examined how MPE-induced SRT in NiO influences the magnetic anisotropy of the FM capping layer in Py/NiO/CoO/MgO(001).²⁷

In our previous study, we successfully grew thin wüstite (FeO) films on MgO(001) and showed how a metallic overlayer modifies the chemical and magnetic properties of the oxide.^{28,29} We noted an exchange interaction between Fe and FeO in the Fe/FeO bilayer structure via observation of the exchange bias field in the hysteresis loops. Despite promising results, the potential application of FeO is limited owing to its low T_N .

This study explores the influence of the proximity of the CoO layer on the magnetic properties of FeO in FeO/CoO heterostructures. Both FeO and CoO insulating oxides crystallize in the rock salt structure. The lattice mismatch between the oxides is less than 1%, which enables the epitaxial growth of the FeO/CoO stack. The ordering temperatures of bulk wüstite and CoO differ significantly. FeO shows an AFM order below 198 K, while the Néel temperature of CoO is 291 K.³⁰ We show that the ordering temperature of FeO can be greatly enhanced owing to the proximity of CoO in the FeO/CoO bilayer. This result confirms that the AFM proximity effect is an effective method for modifying the magnetic properties of the AFM/AFM bilayer without involvement of FMs. Furthermore, we prove that the magnetic proximity of CoO is responsible for the enhancement of the exchange interaction between Fe and FeO in the Fe/FeO/CoO heterostructure.

The samples were prepared under ultra-high vacuum (UHV) conditions using molecular beam epitaxy. A $1 \times 10 \times 10 \text{ mm}^3$ one-side polished MgO(001) single crystal was used as the substrate. The substrates were annealed at 775 K for 1 h before the evaporation process. First, a 5 nm-thick homoepitaxial MgO buffer layer was deposited at 725 K using electron beam evaporation. An additional 20 nm-thick Cr layer deposited at 475 K was used as a buffer for some samples. The CoO layer was grown on the buffer layer by reactive deposition of Co in a molecular oxygen atmosphere under a partial pressure of 1×10^{-6} mbar. Following CoO deposition, a FeO layer was prepared by evaporating Fe in an oxygen atmosphere at 5×10^{-8} mbar. The ^{57}Fe Mössbauer active isotope was used for FeO deposition to enable conversion electron Mössbauer spectroscopy (CEMS) measurements. After the preparation of FeO, the sample was capped with a 3 nm-thick MgO layer. A MgO/FeO/MgO(001) sample was prepared to compare the magnetic properties of wüstite in the FeO/CoO bilayer with a single FeO layer. Finally, a separate sample was grown with a 1 nm-thick Fe layer on top of FeO and capped with 3 nm-thick MgO to examine the influence of the magnetic proximity of CoO on the exchange interaction between Fe and FeO. The epitaxial growth of the layers after each deposition step was confirmed via low-energy electron diffraction (LEED) (not shown).

The magnetic properties of FeO were studied using CEMS. CEMS measurements were performed in a temperature-controlled cryostat under UHV conditions using a channeltron detector, a standard Mössbauer spectrometer, and a $^{57}\text{Co(Rh)}$ source irradiating the sample at normal incidence. Figures 1(a) and 1(b) show the temperature evolution of the CEMS spectra collected for MgO(3 nm)/ ^{57}FeO (1.7 nm)/MgO(001) and MgO(3 nm)/ ^{57}FeO (1.7 nm)/CoO(2 nm)/MgO(001), respectively. For the wüstite layer embedded between MgO, for

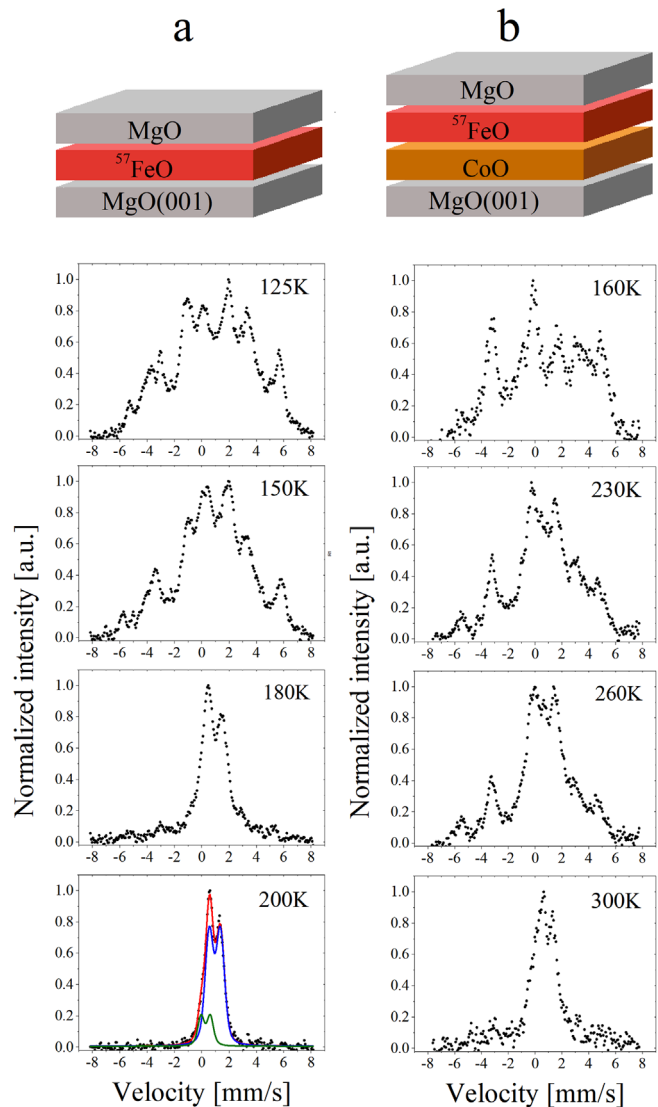


FIG. 1. Temperature evolution of the conversion electron Mössbauer spectra of (a) MgO/ ^{57}FeO /MgO(001) and (b) MgO/ ^{57}FeO /CoO/MgO(001).

temperatures above T_N of FeO (198 K), we noted spectra characteristic for the paramagnetic state. The exemplary spectrum measured at 200 K can be fitted [Fig. 1(a), bottom, red] by two quadrupole doublets identified by their isomer shift (IS) values, describing two different Fe environments. The first site that constitutes 82% of the total spectrum intensity was characterized by IS = 1.06 mm/s and quadrupole splitting (QS) of 0.82 mm/s [Fig. 1(a), blue]; it describes octahedrally coordinated Fe^{2+} atoms in the regular rock salt type wüstite structure.^{29,31} The second component [Fig. 1(a), green] with IS = 0.4 mm/s, QS = 0.67 mm/s, and 18% contribution describes Fe^{3+} atoms in the neighborhood of defects.³¹ For $T = 180 \text{ K}$, we registered a magnetically split spectrum; the magnetic character of the spectra became more pronounced with a further decrease in temperature [Fig. 1(a)]. The low-temperature spectra of FeO are complex and similar to those reported previously,³¹ they consist of

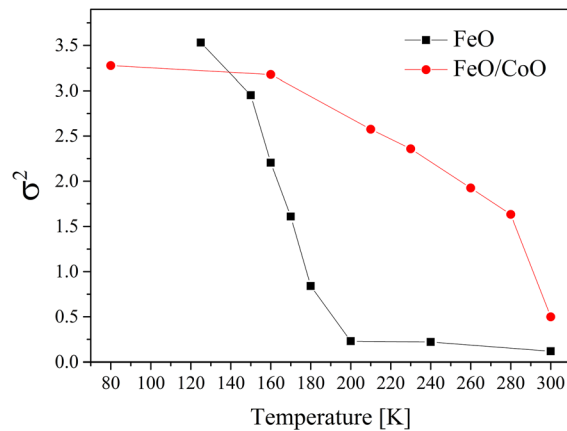


FIG. 2. Dependence of the second moment of the CEMS spectrum on temperature for MgO/FeO/MgO(001) (black squares) and MgO/FeO/CoO/MgO(001) (red circles).

overlapped magnetic sextets that describe regular octahedral and defected/interstitial Fe ions.

Although, due to the complexity, the spectra cannot be unambiguously fitted, it is obvious that below 200 K wüstite undergoes a transition to the AFM phase. To estimate the T_N of the FeO layers, we calculated the second moment (variance, σ^2) of the normalized spectra and plotted its temperature evolution (Fig. 2, black squares). A simple simulation showed that the effective width (given by its second moment) of a complex Mössbauer spectrum with a hyperfine magnetic field (HF) distribution well approximates the average HF experienced by the Fe nuclei below the ordering temperature. Therefore, $\sigma^2(T)$ reflects the temperature dependence of the average HF on the Fe atoms in the FeO layer below T_N , following the temperature variation of the Fe average magnetic moments. The spectra exhibit magnetic character for $T \leq 180$ K; however, the σ^2 of the spectra remains almost unchanged for $T > 180$ K with a small non-zero value resulting from quadrupole splitting in the paramagnetic state. This means that the ordering temperature of FeO in MgO/FeO/MgO is between 180 and

200 K, which is close to the T_N of bulk FeO (i.e., 198 K). Importantly, the magnetic character of the CEMS spectra for the wüstite layer grown on 2 nm-thick CoO was maintained up to significantly higher temperatures [Fig. 1(b)]. The ordering temperature of FeO in MgO/FeO/CoO as determined from $\sigma^2(T)$ dependence was estimated to be between 280 and 300 K, which is close to the T_N of bulk CoO (i.e., 291 K). This result provides direct proof that the proximity of the CoO layer enhances the Néel temperature of FeO.

To determine the T_N of CoO in the FeO/CoO bilayer, we performed x-ray magnetic linear dichroism (XMLD) measurements. X-ray absorption spectra (XAS) were collected at the XAS beamline of the National Synchrotron Radiation Center SOLARIS.³² The absorption Co L_3 -edge spectra were measured as a function of temperature with linearly polarized x rays for two incident angles ($\varphi = 0^\circ$ and $\varphi = 60^\circ$) in the total electron yield (TEY) detection mode by measuring the sample current. Figure 3(a) shows exemplary normalized XAS spectra for a CoO thickness of 2 nm in FeO/CoO, collected under normal ($\varphi = 0^\circ$) and $\varphi = 60^\circ$ x-ray incidence angles at 80 K. We used the L_3 ratio (R_{L_3}), defined as the intensity of the spectrum at 777.3 eV divided by the intensity at 779.9 eV, to quantify the XMLD effect in CoO. The R_{L_3} difference (ΔR_{L_3}) calculated as $\Delta R_{L_3} = R_{L_3}^0 - R_{L_3}^{60}$, where $R_{L_3}^0$ and $R_{L_3}^{60}$ represent the R_{L_3} ratios for incident angles of 0° and 60° , respectively, is a measure of AFM ordering in CoO.³³ We noted positive ΔR_{L_3} values, which indicate the in-plane alignment of CoO AFM spins in FeO/CoO/MgO, similarly to the previous results for CoO/MgO(001), where the in-plane spins direction was attributed to the compressive strain exerted by the substrate.²⁵ With increasing temperature, we observed a monotonic decrease in ΔR_{L_3} up to 300 K, above which the R_{L_3} ratio was almost constant [Fig. 3(b)]. Hence, the Néel temperature of the 2 nm-thick CoO layer in the FeO/CoO bilayer structure can be identified as approximately 300 K. Similar to previous studies, we noted a non-zero ΔR_{L_3} value above the T_N , which indicates the presence of dichroism effects that originate from crystal fields and reveal weak dependence on temperature.^{25,26}

In parallel with the XMLD measurements on CoO, we performed XAS measurements at the Fe L_2 and L_3 edges to examine the x-ray linear dichroism (XLD) effect in the FeO layer. Although we noted a

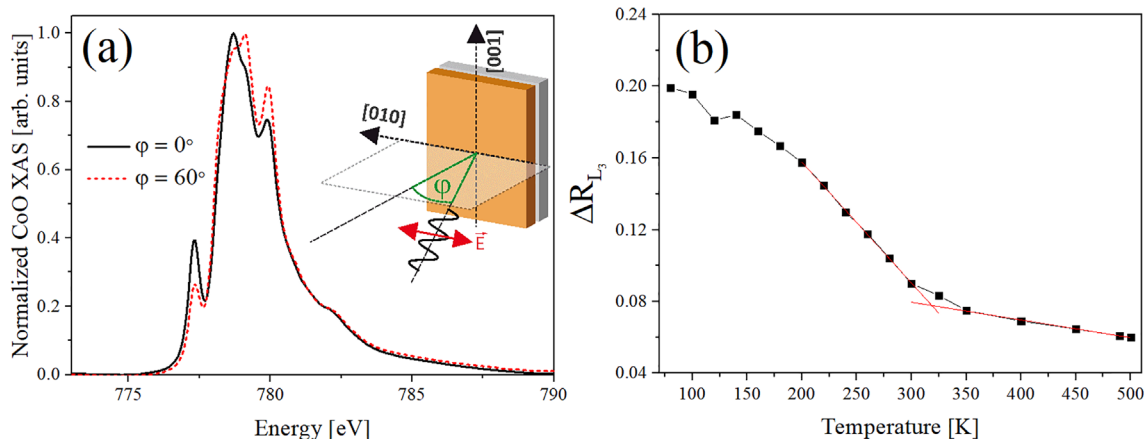


FIG. 3. (a) Co L_3 edge XAS spectra at $\varphi = 0^\circ$ (black solid line) and $\varphi = 60^\circ$ (red dashed line) obtained for FeO/CoO at 80 K. Inset shows the measurement geometry. (b) Temperature dependence of CoO L_3 ratio difference (ΔR_{L_3}) for FeO/CoO (2 nm).

difference in the shape of the XAS spectra for $\varphi = 0^\circ$ and $\varphi = 60^\circ$ (see Fig. 1S in the [supplementary material](#)), we did not observe any dependence of XLD on temperature, especially when passing T_N of FeO in the FeO/CoO bilayer, as determined from CEMS measurements. This indicates that the dichroism effects in the FeO layer are not related to the exchange fields and magnetic moments but are influenced by the local crystal field symmetry. Because the CEMS results unambiguously show the magnetic character of the FeO layer below T_N , we conclude that the lack of the XMLD is related either to its small amplitude, masked by strong natural dichroism, or to the presence of small randomly oriented antiferromagnetic domains in the FeO layer.

The correlation of CEMS and XMLD measurements on the FeO/CoO bilayer indicates that the enhancement of the ordering temperature in FeO is a consequence of the magnetic proximity of CoO. Modification of the magnetic properties of the FeO layer should influence the exchange interaction between the FM layer and FeO in the FM/FeO/CoO multilayer stack. To elucidate this issue, a dedicated sample was prepared with a Fe (1 nm)/FeO (1.7 nm) bilayer grown on a the CoO layer. To study the influence of the CoO thickness on the exchange interaction at the FM/FeO interface, a wedge-shaped CoO layer with a CoO thickness ranging from 0 to 4 nm was prepared. The magnetic properties of this heterostructure were investigated via the magneto-optic Kerr effect (MOKE). The MOKE hysteresis loops were measured in a longitudinal geometry (LMOKE) with an in-plane external magnetic field applied along the [001] direction of the Fe layer. Figure 4 shows exemplary LMOKE hysteresis loops recorded for Fe/FeO (1.7 nm)/CoO (2 nm) (red circles) and Fe/FeO (1.7 nm) (black squares) at 120 K. For the Fe/FeO bilayer grown on the CoO layer, we observed a strong enhancement of the coercive fields [defined as $H_C = (|H_{C1}| + |H_{C2}|)/2$, where H_{C1} and H_{C2} represent the coercive fields of the two branches of the hysteresis loop] and exchange bias, which manifests as a horizontal shift of the hysteresis loop. We noted an H_C of approximately 110 Oe and an exchange bias field [defined as $H_{EB} = (H_{C1} + H_{C2})/2$] of 25 Oe for Fe/FeO, whereas the H_C and H_{EB} extracted for the loop collected for Fe/FeO/CoO were 800 and 190 Oe, respectively. Figure 5 shows the dependence of H_{EB} on temperature obtained from the LMOKE measurements performed for different CoO thicknesses (d_{CoO}) in the Fe/FeO/CoO heterostructure.

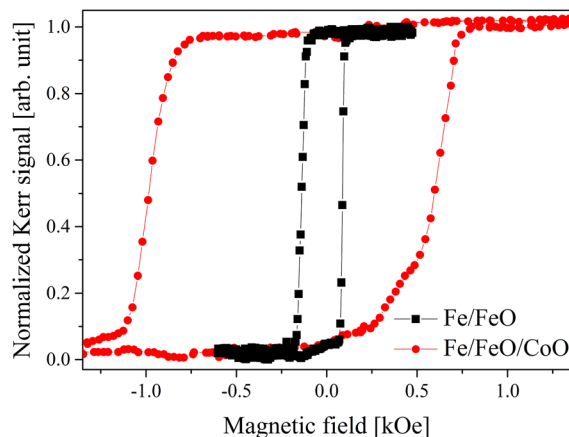


FIG. 4. LMOKE hysteresis loops registered for Fe/FeO (black squares) and Fe/FeO/CoO (red circles) at 120 K.

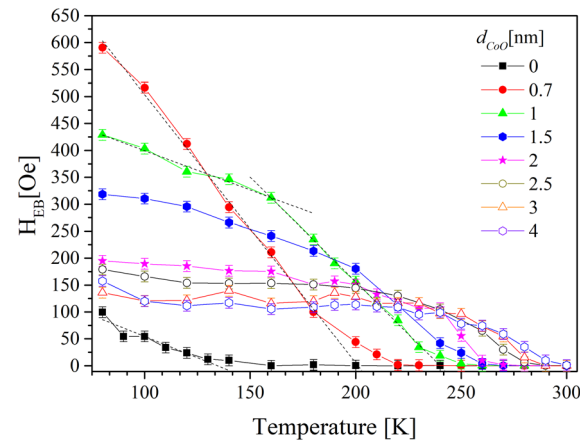


FIG. 5. Evolution of the exchange bias field (H_{EB}) as a function of temperature for FeO (1.7 nm)/CoO for different thicknesses of the CoO layer (indicated in the legend).

The proximity of the CoO layer causes a significant enhancement of the exchange interaction at the Fe/FeO interface. At 80 K, the H_{EB} was increased from 100 to 590 Oe when the Fe/FeO bilayer was deposited on CoO as thin as 0.7 nm (Fig. 5, red).

As the exchange bias field is related to the surface density of the interface energy: $\Delta E = M_{FM}H_{EB}t_{FM}$,³⁴ where M_{FM} and t_{FM} denote the saturation magnetization and thickness of the FM layer, respectively, the areal energy at the Fe/FeO interface in Fe/FeO/CoO was estimated to be approximately 0.1 erg/cm² (assuming the bulk value of M_s for Fe). For the Fe/FeO bilayer, we observed approximately linear temperature dependence of the exchange bias field (Fig. 5, black squares) and a blocking temperature T_B (defined as the temperature at which H_{EB} vanishes) of 160 K. Linear $H_{EB}(T)$ dependence was predicted for AFM with cubic anisotropy by Malozemoff³⁵ and presented experimentally for FM/CoO(NiO) bilayers.^{18,36} We observed a similar characteristic of $H_{EB}(T)$ for the Fe/FeO bilayer deposited on 0.7 nm-thick CoO (Fig. 5, red circles); however, the corresponding value of $T_B = 220$ K was significantly higher than that of the Fe/FeO bilayer. A further increase in d_{CoO} resulted in a decrease in the H_{EB} at 80 K and a monotonic increase in T_B . For the FeO layer deposited on CoO with $d_{CoO} = 2$ nm, for which we determined a T_N of approximately 300 K in CEMS measurements, the T_B was approximately 270 K. This confirms that the T_B of ultrathin AFM can be slightly reduced compared with its Néel temperature.¹⁸ Finally, the value of $T_B = 300$ K registered for Fe/FeO/CoO(4 nm) was approximately twice that obtained for the Fe/FeO bilayer. This indicates that in the studied CoO thickness range, the magnetic properties of the CoO layer are thickness dependent, which is reflected in the strength of the exchange coupling at the Fe/FeO interface. Interestingly, we observed a change in the character of $H_{EB}(T)$ for $d_{CoO} > 0.7$ nm. While at low temperatures, H_{EB} depends only weakly on temperature, a steep $H_{EB}(T)$ dependence is observed above the kink. Temperatures at which we noted the kinks in $H_{EB}(T)$ dependence correspond to the blocking temperatures reported previously for the CoO/Fe bilayers.³⁷ As $H_{EB} \sim (K_{AFM}A_{AFM})^{1/2}$, where K_{AFM} and A_{AFM} are the magnetic anisotropy and exchange stiffness of the AFM layer, respectively, the change in the slope of $H_{EB}(T)$ is related to a reduction in the anisotropy of the FeO layer above the T_B of CoO.³⁴ For the thinnest CoO layer ($t_{CoO} = 0.7$ nm), a significant

reduction in the ordering temperature is expected,³⁷ and the coupling between the CoO and FeO layers does not influence the temperature dependence of the FeO anisotropy, despite the strong enhancement of T_B in Fe/FeO/CoO (0.7 nm). Similar behavior was previously reported for CoO/NiO/NiFe superlattices.²⁴ Finally, for a given temperature, a non-monotonic H_{EB} dependence on d_{CoO} was observed for $T \geq 140$ K, while for temperatures lower than 140 K, a monotonic decrease with an increase in d_{CoO} was noted up to $d_{CoO} = 3$ nm above which H_{EB} saturates (see Fig. 2S in the [supplementary material](#)). Although the $H_{EB} \sim 1/d_{AFM}$ dependence, where d_{AFM} refers to the thickness of the AFM layer, noted at low temperatures was predicted by the random field model,³⁸ Malozemoff's theory does not predict the peak-like structure of H_{EB} vs t_{AFM} observed at elevated temperatures. A non-monotonic $H_{EB}(d_{AFM})$ behavior was reported for FM/CoO bilayers^{37,39} and reproduced by Monte Carlo simulations performed within the framework of the domain-state model of exchange bias⁴⁰ and the generalized Meiklejohn–Bean model.⁴¹ This suggests that at elevated temperatures, the $H_{EB}(d_{CoO})$ dependence of Fe/FeO/CoO mimics the behavior of the FM/CoO layer, while at lower temperatures reflects the properties of Fe/FeO.

In summary, our study demonstrated that the proximity of CoO strongly influences the magnetic properties of the FeO layer. For the wüstite layers grown on 2 nm-thick CoO, the Néel temperature of FeO was increased by 100 K due to the magnetic proximity. This result shows that the limitation of the low ordering temperature of this seemingly application-useless antiferromagnet can be overcome by the antiferromagnetic proximity. Importantly, modification of the magnetic properties of the FeO layer results in the enhancement of the exchange interaction at the Fe/FeO interface in the Fe/FeO/CoO heterostructure. We measured a 500% increase in the exchange bias field for Fe/FeO deposited on the CoO layer compared to H_{EB} in Fe/FeO. Moreover, the blocking temperature for Fe/FeO/CoO (4 nm) was twice as high as that obtained for the Fe/FeO bilayer.

See the [supplementary material](#) for XAS measurements of the Fe $L_{2,3}$ edge and exemplary exchange bias dependence on the CoO thickness at 80 and 160 K.

This publication was developed under the provision of the Polish Ministry of Education and Science project: “Support for research and development with the use of research infrastructure of the National Synchrotron Radiation Centre SOLARIS” under contract nr 1/SOL/2021/2.

We acknowledge SOLARIS Centre for the access to the Beamline XAS, where the measurements were performed.

A.K.-R., M.S. and W.J. were supported by the “Antiferromagnetic proximity effect and development of epitaxial bimetallic antiferromagnets –two routes toward next-generation spintronics” project, which was carried out within the Homing program of the Foundation for Polish Science, co-financed by the European Union under the European Regional Development Fund and by the National Science Centre, Poland (Grant No. 2020/38/E/ST3/00086). M.Ś. was supported by the National Science Centre, Poland (Grant No. 2021/41/B/ST5/01149).

AUTHOR DECLARATIONS

Conflict of Interest

The authors declare that they have no competing interests.

DATA AVAILABILITY

The data that support the findings of this study are available from the corresponding author upon reasonable request.

REFERENCES

- V. Baltz, A. Manchon, M. Tsoi, T. Moriyama, T. Ono, and Y. Tserkovnyak, *Rev. Mod. Phys.* **90**, 015005 (2018).
- D. Hou, Z. Qiu, and E. Saitoh, *NPG Asia Mater.* **11**, 35 (2019).
- P. Wadley, B. Howells, J. Elezny, C. Andrews, V. Hills, R. P. Campion, V. Novak, K. Olejnik, F. Maccherozzi, S. S. Dhesi, S. Y. Martin, T. Wagner, J. Wunderlich, F. Freimuth, Y. Mokrousov, J. Kune, J. S. Chauhan, M. J. Grzybowski, A. W. Rushforth, K. W. Edmonds, B. L. Gallagher, and T. Jungwirth, *Science* **351**, 587 (2016).
- S. Y. Bodnar, L. Šmejkal, I. Turek, T. Jungwirth, O. Gomonay, J. Sinova, A. A. Sapozhnik, H.-J. Elmers, M. Kläui, and M. Jourdan, *Nat. Commun.* **9**, 348 (2018).
- S. DuttaGupta, A. Kurenkov, O. A. Tretiakov, G. Krishnaswamy, G. Sala, V. Krizakova, F. Maccherozzi, S. S. Dhesi, P. Gambardella, S. Fukami, and H. Ohno, *Nat. Commun.* **11**, 5715 (2020).
- L. Baldtrati, A. Ross, T. Niizeki, C. Schneider, R. Ramos, J. Cramer, O. Gomonay, M. Filianina, T. Savchenko, D. Heinze, A. Kleibert, E. Saitoh, J. Sinova, and M. Kläui, *Phys. Rev. B* **98**, 014409 (2018).
- J. Fischer, M. Althammer, N. Vlietstra, H. Huebl, S. T. B. Goennenwein, R. Gross, S. Geprägs, and M. Opel, *Phys. Rev. Applied* **13**, 014019 (2020).
- P. K. Manna and S. M. Yusuf, *Phys. Rep.* **535**, 61 (2014).
- J. J. Hauser, *Phys. Rev.* **187**, 580 (1969).
- O. Rader, E. Vescovo, J. Redinger, S. Blügel, C. Carbone, W. Eberhardt, and W. Gudat, *Phys. Rev. Lett.* **72**, 2247 (1994).
- T. Yang, B. X. Liu, F. Pan, J. Luo, and K. Tao, *J. Phys.: Condens. Matter* **7**, 1121 (1995).
- T. Manago, T. Ono, H. Miyajima, K. Kawaguchi, and M. Sohma, *J. Phys. Soc. Jpn.* **68**, 334 (1999).
- H. Wende, A. Scherz, F. Wilhelm, and K. Baberschke, *J. Phys.: Condens. Matter* **15**, S547 (2003).
- M. A. Tomaz, W. J. Antel, W. L. O'Brien, and G. R. Harp, *J. Phys.: Condens. Matter* **9**, L179 (1997).
- C. Won, Y. Z. Wu, H. W. Zhao, A. Scholl, A. Doran, W. Kim, T. L. Owens, X. F. Jin, and Z. Q. Qiu, *Phys. Rev. B* **71**, 024406 (2005).
- K. Lenz, S. Zander, and W. Kuch, *Phys. Rev. Lett.* **98**, 237201 (2007).
- J. van Lierop, K.-W. Lin, J.-Y. Guo, H. Ouyang, and B. W. Southern, *Phys. Rev. B* **75**, 134409 (2007).
- P. J. van der Zaag, Y. Ijiri, J. a Borchers, L. F. Feiner, R. M. Wolf, J. M. Gaines, R. W. Erwin, and M. a Verheijen, *Phys. Rev. Lett.* **84**, 6102 (2000).
- V. Skumryev, S. Stoyanov, Y. Zhang, G. Hadjipanayis, D. Givord, and J. Nogués, *Nature* **423**, 850 (2003).
- A. T. Hindmarch, K. J. Dempsey, J. P. Morgan, B. J. Hickey, D. A. Arena, and C. H. Marrows, *Appl. Phys. Lett.* **93**, 172511 (2008).
- J. M. Vargas, J. Gómez, R. D. Zysler, and A. Butera, *Nanotechnology* **18**, 115714 (2007).
- C. A. Ramos, D. Lederman, A. R. King, and V. Jaccarino, *Phys. Rev. Lett.* **65**, 2913 (1990).
- M. Takano, T. Terashima, Y. Bando, and H. Ikeda, *Appl. Phys. Lett.* **51**, 205 (1987).
- M. J. Carey, A. E. Berkowitz, J. A. Borchers, and R. W. Erwin, *Phys. Rev. B* **47**, 9952 (1993).
- J. Zhu, Q. Li, J. X. Li, Z. Ding, J. H. Liang, X. Xiao, Y. M. Luo, C. Y. Hua, H. J. Lin, T. W. Pi, Z. Hu, C. Won, and Y. Z. Wu, *Phys. Rev. B* **90**, 054403 (2014).
- Q. Li, J. H. Liang, Y. M. Luo, Z. Ding, T. Gu, Z. Hu, C. Y. Hua, H.-J. Lin, T. W. Pi, S. P. Kang, C. Won, and Y. Z. Wu, *Sci. Rep.* **6**, 22355 (2016).
- M. Yang, Q. Li, A. T. N. Diaye, Q. Y. Dong, N. Gao, E. Arenholz, C. Hwang, Y. Z. Wu, and Z. Q. Qiu, *J. Magn. Magn. Mater.* **460**, 6–11 (2018).
- A. Koziol-Rachwał, T. Ślęzak, T. Nozaki, S. Yuasa, and J. Korecki, *Appl. Phys. Lett.* **108**, 041606 (2016).
- A. Koziol-Rachwał, W. Janus, M. Szpytma, P. Drózd, M. Ślęzak, K. Matlak, M. Gajewska, and T. Ślęzak, *Appl. Phys. Lett.* **115**, 141603 (2019).
- J. R. Singer, *Phys. Rev.* **104**, 929 (1956).

- ³¹C. Wilkinson, A. K. Cheetham, G. J. Long, P. D. Battle, and D. A. O. Hope, *Inorg. Chem.* **23**, 3136 (1984).
- ³²M. Zając, T. Gieła, K. Freindl, K. Kollbek, J. Korecki, E. Madej, K. Pitala, A. Koziol-Rachwał, M. Sikora, N. Spiridis, J. Stępień, A. Szkudlarek, M. Ślęzak, T. Ślęzak, and D. Wilgocka-Ślęzak, *Nucl. Instrum. Methods Phys. Res. Sect. B* **492**, 43 (2021).
- ³³G. Van Der Laan, E. Arenholz, R. V. Chopdekar, and Y. Suzuki, *Phys. Rev. B* **77**, 064407 (2008).
- ³⁴J. Nogués and I. K. Schuller, *J. Magn. Magn. Mater.* **192**, 203 (1999).
- ³⁵A. P. Malozemoff, *J. Appl. Phys.* **63**, 3874 (1988).
- ³⁶M. Ślęzak, P. Drózdź, A. Koziol-Rachwał, K. Matlak, J. Korecki, M. Zając, and T. Ślęzak, *Acta Phys. Pol. A* **137**, 44 (2020).
- ³⁷J. Gurgul, E. Młynczak, A. Koziol-Rachwał, K. Matlak, K. Freindl, E. Madej, N. Spiridis, T. Ślęzak, and J. Korecki, *Phys. Rev. B* **96**, 104421 (2017).
- ³⁸A. P. Malozemoff, *Phys. Rev. B* **37**, 7673 (1988).
- ³⁹P. J. Van Der Zaag, A. R. Ball, L. F. Feiner, R. M. Wolf, and P. A. A. Van Der Heijden, *J. Appl. Phys.* **79**, 5103 (1996).
- ⁴⁰U. Nowak, A. Misra, and K. D. Usadel, *J. Appl. Phys.* **89**, 7269 (2001).
- ⁴¹C. Binek, A. Hochstrat, and W. Kleemann, *J. Magn. Magn. Mater.* **234**, 353 (2001).